Accepted Manuscript

Exploiting topology-directed nanoparticle disassembly for triggered drug delivery

Maria C. Arno, Rebecca J. Williams, Panagiotis Bexis, Anaïs Pitto-Barry, Nigel Kirby, Andrew P. Dove, Rachel K. O'Reilly

Exploiting topology-directed nanoparticle disassembly for triggered drug delivery

Maria C. Arno[‡,a,b] Rebecca J. Williams[‡,a] Panagiotis Bexis,[a,b] Anaïs Pitto-Barry,[a] Nigel Kirby,[c] Andrew P. Dove[a,b] and Rachel K. O'Reilly[a,b]**

[a]University of Warwick, Department of Chemistry, Gibbet Hill Road, Coventry CV4 7AL, UK.

[b]University of Birmingham, School of Chemistry, Edgbaston, Birmingham, B15 2TT, UK.

[c]Australian Synchrotron, 800 Blackburn Road, Clayton, Victoria 3168, Australia.

‡ These authors contributed equally.

*E-mail: r.oreilly@bham.ac.uk; a.dove@bham.ac.uk

KEYWORDS: graft copolymers, cyclic polymers, disulfide linker, acetal linker, topology-controlled particle disassembly

Abstract

The physical properties of cyclic and linear polymers are markedly different; however, there are few examples which exploit these differences in clinical applications. In this study, we demonstrate that self-assemblies comprised of cyclic-linear graft copolymers are significantly more stable than the equivalent linear-linear graft copolymer assemblies. This difference in stability can be exploited to allow for triggered disassembly by cleavage of just a single bond within the cyclic polymer backbone, *via* disulfide reduction, in the presence of intracellular levels of $_L$-glutathione. This topological effect was exploited to demonstrate the first example of topology-controlled particle disassembly for the controlled release of an anti-cancer drug

in vitro. This approach represents a markedly different strategy for controlled release from polymer nanoparticles and highlights for the first time that a change in polymer topology can be used as a trigger in the design of delivery vehicles. We propose such constructs, which demonstrate disassembly behavior upon a change in polymer topology, could find application in the targeted delivery of therapeutic agents.

Introduction

Polymer topology can exert significant influence over the properties and potential applications of a polymeric material. Among the range of accessible topologies, cyclic polymers have drawn considerable attention as a consequence of the unique behavior they exhibit in comparison to their linear counterparts.[1-8] While significant progress has been made towards understanding these fundamental property differences, there are comparatively few reports that exploit these differences in specific applications. Nevertheless, polymers with a cyclic topology have shown great promise as potential drug and gene delivery vehicles, often exhibiting greater efficacy, *e.g.* higher gene transfection efficiencies,[9-10] longer *in vivo* circulation times,[11] and higher cancer cell uptake,[11-13] than their linear counterparts. Furthermore, amphiphilic cyclic polymers display markedly different self-assembly behavior compared to linear amphiphilic polymers,[6] with cyclization shown to affect the dimensions,[14] morphology,[15-17] temperature and salt tolerance,[18-19] and degradation[14] of polymer self-assemblies.

The selective delivery of therapeutic compounds from polymer nanoparticles shows promise for the treatment of cancer and other diseases. Controlled release of a compound at the site of action is desirable to maximize efficacy, minimize side-effects and frequency of administration. As such, triggered particle disassembly has been studied as a means to control payload release.[20-21] Whilst numerous stimuli including temperature[22-23] and light[24] have been

2

exploited to trigger particle disassembly, these are generally not suitable for *in vivo* applications given the inability to precisely control these factors within the cell. Thus, polymer degradation is the generally favored mechanism for *in vivo* particle disassembly and cargo release. Degradation may be selective or non-selective, for example, the hydrolysis of ester linkages is non-specific and occurs under all physiological conditions, while the reduction of disulfide bonds in the presence of the biological reducing agent L-glutathione (GSH) occurs primarily in intracellular environments as a consequence of the 100-fold increase of GSH in intracellular environments compared to extracellular environments.[25-26] Indeed, the difference in intracellular and extracellular GSH concentration has been elegantly exploited for the disassembly of polymeric constructs through the cleavage of disulfide crosslinks, which has been coupled to the release of a range of payloads.[27-28] However, in all instances of particle disassembly through degradation or breakage of crosslinks, consideration must be given to the resulting degradation products, which may differ significantly in chemical structure, molar mass, solubility, and therefore toxicity and retention, compared to the original polymer.

To overcome this limitation, we designed a new class of responsive constructs that can undergo a topological change and disassembly process in response to a reducing (intracellular) environment. We report the first instance of topology-controlled particle disassembly *in vitro*, triggered by a switch in polymer topology from cyclic to linear, where the disassembled and original polymers vary only in topology. Inspired by the observation that self-assemblies of cyclic-linear graft copolymers (with a cyclic core and linear arms) were significantly more stable than equivalent linear-linear graft copolymer assemblies (with a linear core and linear arms), we hypothesized that this topology effect could be exploited to trigger particle disassembly through incorporation of a cleavable disulfide linkage in the cyclic polymer backbone. Upon disulfide cleavage, the cyclic-linear graft copolymer

assembly switches to an unstable linear graft copolymer assembly, which disassembles. Importantly, disulfide cleavage and subsequent particle disassembly can be triggered in the presence of intracellular levels of the cellular reducing agent L-glutathione. To demonstrate that the topology switch is independent from the cleavable linker selected, an acid-sensitive acetal linker was incorporated in the cyclic polymer structure, and the topology-directed disassembly was triggered by acidic pH. This approach represents a significant breakthrough in the development of new strategies for *in vivo* particle disassembly and the selective delivery of therapeutic agents, as well as expanding the potential applications of cyclic polymers.

Materials and methods

Materials

1,8-Diazabicyclo[5.4.0]undec-7-ene (DBU) was dried over CaH_2, distilled and stored under inert atmosphere. 1,4-butanediol and 1,3-propanediol were dried and stored over 3 Å molecular sieves. RAFT CTA-functional carbonate and 5-methyl-5-ethoxycarbonyl-1,3-dioxan-2-one monomers were synthesized as previously reported and dried over 3 Å molecular sieves in dry CH_2Cl_2.[29-30] 4-pentynoic anhydride was prepared according to the literature.[13,31] AIBN (2,2'-azo-bis(isobutyronitrile)) was recrystallized twice from methanol and stored in the dark at 4 ˚C. CH_2Cl_2 was purified over Innovative Technology SPS alumina solvent columns and degassed before use. Nanopure water with a resistivity of 18.2 MΩ·cm was prepared using a Millipore Simplicity UV ultrapure water purification system. All other solvents and chemicals were obtained from Sigma-Aldrich or Fisher Scientific and used as received. For the biological studies, A549 cells were purchased from Public Health England, UK. F-12K (Kaighn's) medium was purchased from Gibco, fetal bovine serum (FBS) was

acquired from Sigma-Aldrich, penicillin/streptomycin (pen/strep) antibiotic solution was acquired from Fisher Scientific.

Synthesis of RAFT CTA-functional polycarbonate

1,8-Diazabicyclo[5.4.0]undec-7-ene (DBU) (38 mg, 0.25 mmol) was added to a solution of the appropriate equivalents of RAFT CTA-functional carbonate (1 g, 2.5 mmol), 5-methyl-5-ethoxycarbonyl-1,3-dioxan-2-one (0.47 g, 2.5 mmol) and 1,4-butanediol (0.018 g, 0.2 mmol) or 1,3-propanediol (0.011 g, 0.2 mmol) in dry CH_2Cl_2 (20 mL) and stirred at room temperature. After the desired amount of time the polymerization was quenched by the addition of Amberlyst 15 H^+ ion exchange resin. The resin was removed by filtration, the solution concentrated and the polymer precipitated in cold diethyl ether. The unreacted monomers and residual DBU were removed by column chromatography (silica, 100% CH_2Cl_2, then 100% ethyl acetate, yield = 65%).[32] ^{1}H NMR (400 MHz, $CDCl_3$, ppm): δ = 7.31-7.26 (m, $4H_{backbone-1}$, Ar), 5.11 (m, $2H_{backbone-1}$, OCH_2Ar), 4.59 (m, $2H_{backbone-1}$, SCH_2Ar), 4.28 (m, $8H_{backbone-1+2}$, $C=OOCH_2C(CH_3)CH_2O$), 4.17 (m, $2H_{backbone-2}$, OCH_2CH_3), 4.11 (m, $4H_{end-group}$, OCH_2CH_2), 3.37 (m, $2H_{backbone-1}$, SCH_2CH_3), 1.73 (m, $4H_{end-group}$, OCH_2CH_2), 1.35 (m, $3H_{backbone-1}$, SCH_2CH_3), 1.24 (m, $6H_{backbone-1+2}$, CCH_3), 1.21 (m, $3H_{backbone-2}$, OCH_2CH_3). SEC ($CHCl_3$ + 0.5% NEt_3, PS standards): M_n (SEC) = 6.0 kg mol^{-1}, $Đ_M$ = 1.18.

End-group functionalization

Pyridine (0.12 g, 1.5 mmol) was added to a solution of RAFT CTA-functional polycarbonate (1 g, 0.15 mmol), 4-pentynoic anhydride[32] (0.88 g, 4.5 mmol) and DMAP (55 mg, 0.45 mmol) in dry CH_2Cl_2 (30 mL) and stirred under nitrogen for 36 h. The solution was washed with saturated $NaHSO_4$ (2 × 50 mL) and saturated $NaHCO_3$ (2 × 50 mL) and the organic layer dried over $MgSO_4$. Solvent was removed *in vacuo*, the polymer residue dissolved in the minimum amount of $CHCl_3$ and precipitated into petroleum ether 40-60 °C three times (Yield = 82%).[32] ^{1}H NMR (400 MHz, $CDCl_3$, ppm): δ = 7.31-7.26 (m, $4H_{backbone-1}$, Ar), 5.11 (m,

$2H_{backbone-1}$, OCH_2Ar), 4.59 (m, $2H_{backbone-1}$, SCH_2Ar), 4.28 (m, $8H_{backbone-1+2}$, C=OOCH_2C(CH$_3$)CH_2O), 4.17 (m, $2H_{backbone-2}$, OCH_2CH$_3$), 4.11 (m, $4H_{end-group}$, OCH_2CH$_2$), 3.87 (m, $2H_{backbone-1}$, SCH_2CH$_3$), 2.55 (m, $4H_{end-group}$, CH_2CH$_2$CCH), 2.50-2.42 (m, $4H_{end-group}$, CH$_2$CH_2CCH), 1.97 (m, $2H_{end-group}$, CH), 1.73 (m, $4H_{end-group}$, OCH$_2$CH_2), 1.34 (m, $3H_{backbone-1}$, SCH$_2$CH_3), 1.24 (m, $6H_{backbone-1+2}$, CCH_3), 1.22 (m, $3H_{backbone-2}$, OCH$_2$CH_3). SEC (CHCl$_3$ + 0.5% NEt$_3$, PS standards): M_n (SEC) = 7.4 kg mol^{-1}, $Đ_M$ = 1.17.

Synthesis of azides small molecules

Caution: Small organic azides are potentially explosive and must be handled with care, particularly in concentrated forms and/or in large quantities. Keep away from sources of heat, pressure, light, shocks and strong acids. Bis-(azidoethyl)disulfide was prepared according to literature procedures (Yield: 80%).[13,33] ^{1}H NMR (400 MHz, CDCl$_3$, ppm): δ = 3.59 (t, 4H, N$_3$CH_2, $^3J_{H-H}$ = 6.7 Hz), 2.86 (t, 4H, SCH_2, $^3J_{H-H}$ = 6.7 Hz). ^{13}C NMR (100 MHz, CDCl$_3$, ppm): δ = 50.0 (N$_3$$CH_2$), 37.7 (S$CH_2$).

1,8-diazidooctane was prepared according to literature procedures (Yield: 78%).[34-35] ^{1}H NMR (300 MHz, CDCl$_3$, ppm): δ = 3.25 (t, 4H, N$_3$CH_2, $^3J_{H-H}$ = 6 Hz), 1.64-1.55 (m, 4H, N$_3$CH$_2$CH_2), 1.34 (m, 8H, CH_2). ^{13}C NMR (300 MHz, CDCl$_3$, ppm): δ = 52.5 (N$_3$$CH_2$), 29.1 (N$_3CH_2$$CH_2$), 28.9 ($CH_2$), 26.7 ($CH_2$).

2,2-bis(2-azidoethoxy)propane was prepared as described below. Imidazole-1-sulfonyl azide hydrochloride was prepared according to a literature procedure.[36] 2-[1-(2-Amino-ethoxy)-1-methyl-ethoxy]-ethylamine (AEE) was prepared following a literature procedure.[37] Imidazole-1-sulfonyl azide hydrochloride (2.6 g, 12.40 mmol) was then added to a solution of AEE (1 g, 6.17 mmol) in MeOH (20 mL). Potassium carbonate (2.6 g, 19 mmol) and copper(II) sulfate pentahydrate (0.015 g, 0.062 mmol) were then added to the mixture. The solution was stirred at room temperature overnight, then concentrated and diluted with water (20 mL). The product was then extracted with EtOAc (100 mL), washed with brine (3

× 50 mL), and dried over MgSO$_4$. Flash chromatography was used for purification (90:10 hexane:EtOAc) to obtain a clear viscous liquid (Yield: 63%). ^{1}H NMR (300 MHz, CDCl$_3$, ppm): δ = 3.64 (t, 4H, N$_3$CH_2, $^3J_{H-H}$ = 6 Hz), 3.36 (t, 4H, N$_3$CH$_2$CH_2O, $^3J_{H-H}$ = 6 Hz), 1.39 (s, 6H, CH_3). ^{13}C NMR (300 MHz, CDCl$_3$, ppm): δ = 100.61 (*C*), 60.17 (N$_3$CH$_2$*C*H$_2$O), 51.1 (N$_3$*C*H$_2$), 24.76 (*C*H$_3$). Mass = [M$^+$ + Na$^+$] 236.7.

Cyclization via the copper-catalyzed azide-alkyne cycloaddition

A solution of *N,N,N',N''*-pentamethyldiethylenetriamine (PMDETA) in toluene (0.15 g, 0.9 mmol, 0.002 M) was bubbled with nitrogen for 1 h. Cu(I)Br (0.12 g, 0.83 mmol) was added and the solution bubbled for a further 30 min. In a separate ampoule a solution of alkyne terminated RAFT CTA-functional polycarbonate (0.06 g, 0.008 mmol) and a diazide linker (1.7 mg, 0.008 mmol) in toluene (1 mM) was degassed *via* 3 freeze-pump-thaw cycles. The degassed solution was then transferred into a gas-tight glass syringe and added at a rate of 0.3 mL/h to the solution of PMDETA and Cu(I)Br whilst stirred under nitrogen. After complete addition the solution was stirred for a further 3 h, then washed with saturated NaHCO$_3$ (3 × 50 mL) and brine (3 × 50 mL) and the organic layer dried over MgSO$_4$. Toluene was removed *in vacuo* and the polymer residue was dissolved in CH$_2$Cl$_2$ (100 mL) and stirred in the presence of Cuprisorb beads overnight. The beads were removed *via* filtration and the polymer was precipitated into petroleum ether 40-60 ˚C (50 mL) three times (Yields = 45-51%). ^{1}H NMR (400 MHz, CDCl$_3$, ppm): δ = 7.31-7.25 (m, 4H$_{backbone-1}$, Ar), 5.12 (m, 2H$_{backbone-1}$, OCH_2Ar), 4.59 (m, 2H$_{backbone-1}$, SCH_2Ar), 4.28 (m, 8H$_{backbone-1+2}$, C=OOCH_2C(CH$_3$)CH_2O), 4.17 (m, 2H$_{backbone-2}$, OCH_2CH$_3$), 4.12 (m, 4H$_{end-group}$, OCH_2CH$_2$), 3.37 (m, 2H$_{backbone-1}$, SCH_2CH$_3$), 3.14-2.59 (m, 12H$_{end-group}$, CH_2SSCH_2 + CH_2CH$_2$CCH + CH$_2$CH_2CCH), 1.73 (m, 4H$_{end-group}$, OCH_2CH$_2$), 1.35 (m, 3H$_{backbone-1}$, SCH$_2$CH_3), 1.24 (m, 6H$_{backbone-1+2}$, CCH_3), 1.22 (m, 3H$_{backbone-2}$, OCH$_2$CH_3). SEC (CHCl$_3$ + 0.5% NEt$_3$, PS standards): M_n (SEC) = 6.2 kg mol^{-1}, $Đ_M$ = 1.16.

General procedure for RAFT polymerizations

The appropriate equivalents of RAFT CTA-functional cyclic (0.05 g, 0.008 mmol) or linear polycarbonate (0.05 g, 0.007 mmol), AIBN (0.5 eq. to total RAFT CTA groups) and 4-Acryloylmorpholine (0.76 g, 5.4 mmol) were loaded into a dry ampoule and dissolved in CHCl$_3$ (1.5 mL). The reaction mixture was degassed *via* 4 freeze-pump-thaw cycles and refilled with nitrogen. The polymerization was initiated by immersion of the ampoule into an oil bath at 70 ˚C. After the desired length of time the polymerization was quenched by immersion of the ampoule in liquid nitrogen. Monomer conversions were kept below 50% to minimize graft-graft coupling.

General procedure for particle preparation

Assemblies were prepared using the solvent switch method or the direct dissolution method. In the first case, the relevant polymer was dissolved in THF at 10 mg/mL. 18.2 MΩ·cm water (20 mL) was added to the stirred solution *via* a peristaltic pump at a rate of 0.6 mL/h. After complete water addition, THF was removed *via* exhaustive dialysis (6-8 kDa MWCO) against 18.2 MΩ·cm water for 3 days to yield a final concentration of *ca*. 0.5 mg/mL. No loss of polymer was observed after dialysis under these conditions. In the direct dissolution method, the relevant polymer was dissolved in 18.2 MΩ·cm water to reach the desired concentration (from 0.25 to 2 mg/mL) and analysed directly after.

General procedure for particle preparation via thin film hydration

The relevant polymer was dissolved in CHCl$_3$ (1 mg/mL) in a round bottom flask. CHCl$_3$ was removed *in vacuo* to leave a thin polymer film coating the inside of the flask. 18.2 MΩ·cm water was carefully added down the side of the flask to prevent disruption of the polymer film, which was left to hydrate for 16 h to give a final polymer concentration of *ca*. 0.5 mg/mL.

Determination of cmc via fluorescence spectroscopy

73 µL of a stock solution of pyrene in acetone (2.47×10^{-6} M) was added to several vials and the acetone subsequently evaporated. The cyclic and linear assemblies were prepared *via* direct dissolution in 18.2 MΩ·cm water, with concentrations from 0.0003 to 2 mg/mL. 300 µL of each polymer solution was added to a pyrene containing vial and stirred overnight to give a final pyrene concentration of 6×10^{-7} M. Excitation spectra were recorded in the range λ_{ex} = 300-375 nm and λ_{em} = 390 nm. A clear shift in the excitation spectra of pyrene of the excitation maxima from *ca.* 339 to 335 nm is observed when pyrene enters a hydrophobic environment. Comparison of the intensity of these two signals ($I_{339}/I_{334.5}$) over a range of polymer concentrations allows determination of the cmc; where the cmc was taken as the inflection point in the plot of $I_{339}/I_{334.5}$ *vs* polymer concentration.

Encapsulation of small molecules

The relevant polymer was dissolved in 2 mL of DMSO at a concentration of 10 mg/mL. 20 wt% of the small molecule (BODIPY-FL, Camptothecin) was then added to the solution and stirred for 30 min to achieve a homogeneous solution. 20 mL of 18.2 MΩ·cm water was then added to the solution and left to stir overnight. Exhaustive dialysis (6-8 kDa MWCO) against 18.2 MΩ·cm water for 3 days was then used to remove any un-encapsulated dye/drug. The drug loading was optimized using different feeding ratios (5, 10, 20, 40% w/w of drug:polymer) and it was observed that a feeding ratio of 20% would achieve the highest encapsulation efficiency (70%). Encapsulation efficiency (EE) was calculated using the following equation:

$$EE = \frac{Amount\ of\ drug\ loaded\ in\ the\ assemblies}{Amount\ of\ drug\ added\ during\ assembly} \times 100$$

where the amount of drug was measured *via* fluorescence spectroscopy. Cyclic or linear assemblies were dissolved in DMSO to a concentration of 1 mg/mL. The drug loading was calculated for all the cyclic polymers independently and for the linear 2 polymer by fluorescence measurements using a plate reader. The solution of assemblies (40 µL) and

DMSO (10 µL) were pipetted into a black flat bottom 96 well plate and read on a BMG Labtech FLUOstar OPTIMA plate reader (λ_{ex} = 370 nm λ_{em} = 428 nm). Three samples were read and the fluorescence averaged. Control curves were constructed by dissolving blank assemblies as described above and adding known amounts of drug.

Drug release studies

The relevant polymer (2 mL, 1 mg/mL) was incubated with either 10 µM or 10 mM of L-glutathione and the vial was placed in a shaking incubator (60 rpm) at 37 °C. Time points were taken every 2 hours, up to 16 h, and the drug concentration was measured using a Spectrofotometer FS5 by Edinburgh Instruments (λ_{ex} = 370 nm λ_{em} = 428 nm).

Cell viability studies

A549 cells were cultured in F-12K (Kaighn's) medium with the addition of 10% FBS and 1% pen/strep at 37 °C, 5% CO_2. For the viability experiments, cells were seeded on 24 wells plates at a seeding density of 10000 cells/mL and let adhere and proliferate for 72 h. Culture medium was then replaced with an increasing concentration of linear or cyclic assemblies (from 0 to 2 mg/mL), and linear or cyclic assemblies encapsulating camptothecin (from 0 to 250 nM of camptothecin in the case of cyclic assemblies and from 0 to 7 nM in the case of linear assemblies). Briefly, the cyclic polymers (20 mg) were dissolved in DMSO (2 mL), then camptothecin (4 mg) was added. After 30 min. under stirring 18 mL of water was added to the solution, which was then dialysed to remove DMSO. 20 mL of the particles solution was obtained after dialysis, with a drug loading of 0.14 mg of camptothecin per mg of polymer (2.8 mg camptothecin per 20 mg of polymer and therefore 0.8×10^{-5} mols and 0.4×10^{-3} M). This solution was further diluted (0.4×10^{-4} M) in cell culture medium and this was used as a stock solution for the camptothecin concentration range used in the cell studies. Experiments were performed in triplicate, seeding equal number of cells on three different wells and analysing the viability data from each well. Time points were taken at 24 and 72 h

of incubation, after removing the polymer solutions and washing the wells with PBS (3×1 mL). Viability was assessed by counting the living cells in each well after trypsinization. Specifically, each well was incubated with 0.5 mL of trypsin for 5 min at 37 ˚C, 5% CO_2. Trypsin was then diluted with culture medium (1:1) and cells were centrifuged at 2000 rpm for 5 min to obtain a pellet. The cell pellet was then re-dispersed in fresh medium (1 mL), and 50 µL of this solution diluted 1:1 with trypan blue. 10 µL of the cell solution was then placed in each counting chamber of a haemocytometer and the total number of cells was obtained using a Countess II FL Automated Cell Counter. Cell viability is expressed as a percentage against the control (polymer concentration = 0 mg/mL). PrestoBlue cell proliferation assay was also used to assess the cytotoxicity of the cyclic and linear polymers, following the suppliers' instructions. However it was observed that cyclic 1i was interfering with the assay, which is sensitive to thiols and other reducing agents,[38] and therefore cell counting was selected as the preferred method to determine cell viability and obtain comparable data between the different cyclic-linear polymers.

Internalization of the assemblies by A549 cells

A549 cells were cultured as described in the previous paragraph. For the experiments, cells were seeded at a seeding density of 10000 cells/mL on EtOH sterilized circular glass slides (19 mm in diameter) placed on 12 wells plates. Cells were let adhere and proliferate for 72 h. Culture medium was then replaced with 0.1 mg/mL or 0.3 mg/mL of polymer (cyclic or linear) encapsulating BODIPY-FL, diluted with the same F-12K (Kaighn's) medium. Cells were incubated at 37 ˚C, 5% CO_2 for 4 h, after which the medium was discarded and cells were washed with PBS (3×1 mL). Experiments were performed in triplicate. Cells were then fixed with a 4% paraformaldehyde solution in PBS for 10 min at room temperature, then washed with PBS (3×1 mL). Cells were then permeabilized with a solution of Triton X-100 for 20 min at room temperature and washed with PBS (3×1 mL, 5 min each). Nuclei were

then stained with DAPI (15 µL in 20 mL of PBS) for 5 min, washed with PBS (3 × 1 mL) and finally stored in the dark at 4 ˚C overnight. Imaging was performed using a Zeiss LSM 880 inverted confocal microscope. DAPI (λ_{ex} = 358 nm, λ_{em} = 461 nm) was excited with a 405 nm laser, and BODIPY-FL (λ_{ex} = 503 nm, λ_{em} = 512 nm) with a 488 laser. At least ten pictures per glass slide were taken, covering the whole sample area.

Results and discussion

Amphiphilic cyclic-linear and linear-linear graft copolymers, **1** and **2**, (Figure 1) were prepared as previously reported *via* a combination of ring-opening (ROP) and reversible addition-fragmentation chain transfer (RAFT) polymerization.[30,32] Cyclization was achieved *via* copper-catalyzed azide-alkyne cycloaddition and utilized three different linking agents. The disulfide- and acetal-containing linkers were selected to introduce a reduction- and pH-sensitive cleavable functionality to the cyclic polymer backbone (cyclic-linear graft copolymers **1i** and **1ii**, respectively). A non-responsive, alkyl linker, was also selected as a control for non-triggered disassembly (cyclic-linear graft copolymer **1iii**). Graft copolymer arms were composed of poly(*N*-acryloylmorpholine) (PNAM), with degrees of polymerisation of *ca.* 19. As a result of experimental error, the molecular weights and dispersities of the polymers considered in this study vary between the different polymerisations performed, and hence the ratio between the hydrophobic and hydrophilic weight fractions may be different. Full characterization details for all of the polymers are available in the Supporting Information (Figures S1-S22 and Table S1).

12
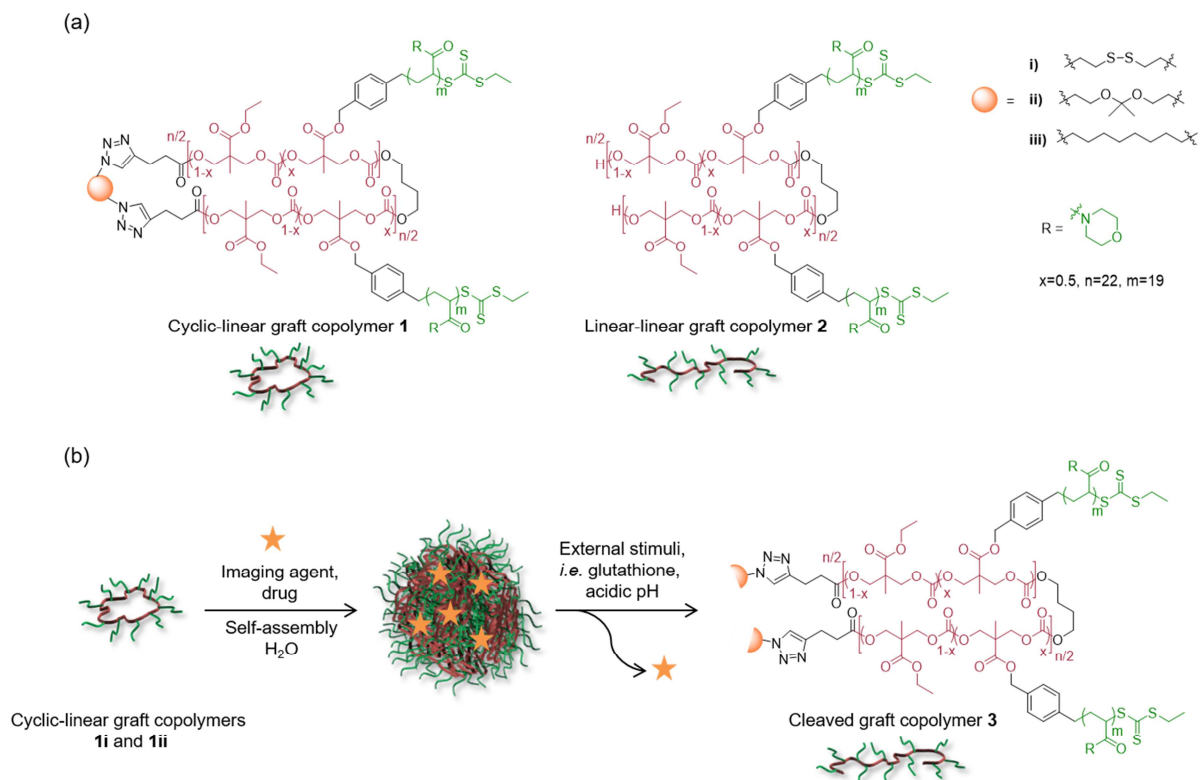
Figure 1. (a) Cyclic-linear and linear-linear (**1** and **2**) PNAM graft copolymers, where **1** is cyclized with two responsive linkers to give **1i** and **1ii** and one non-responsive linker to give **1iii**; (b) Self-assembly of **1** in the presence of an imaging agent or a drug and subsequent particle disassembly and cargo release triggered by external stimuli (in the case of **1i** and **1ii**), to give cleaved linear graft copolymer **3**.

Self-assembly of PNAM cyclic-linear and linear-linear graft copolymers **1i** (with the disulfide linkage) and **2,** respectively, was studied with an emphasis on probing the relative stabilities of the assemblies. Three methods of polymer self-assembly were investigated; direct dissolution in water (18.2 MΩ·cm), solvent switch from THF to water and thin film hydration, all to give [polymer] = *ca*. 0.5 mg/mL. For assemblies of cyclic-linear graft copolymer **1i**, well-defined aggregates with consistent values of D_h (150 - 170 nm) were produced each time (Table 1, Figure 2 and S23). In contrast, a large disparity in particle size was observed for linear-linear graft copolymer **2** for the different assembly techniques. Large structures ($D_h > 100$ nm) were observed for direct dissolution and solvent switch (Table 1, Figure 2 and S23), whereas small species consistent with unimers ($D_h = 7$ nm) were observed following thin film hydration, suggesting the absence of aggregation or that the resulting

13

assemblies were unstable (Table 1, Figure S23). Additionally, aggregates of linear-linear graft copolymer **2** exhibited significantly different particle sizes (D_h = 200-600 nm) and broader dispersities (PD *ca*. 0.4) for each repeat by DLS (Figure S23). The aggregates formation was further probed by determination of critical micelle concentration (cmc) (0.09 g/L for cyclic-linear graft copolymer **1i** and 0.23 g/L for linear-linear graft copolymer **2**) (Table 1, Figure 2). However, while the cmc is indicative of the concentration at which the polymers aggregate, it gives no information on the stability and dynamic nature of the aggregation process. Thus, the stability of the particles to changes in polymer concentration was investigated by DLS. Assemblies of linear-linear graft copolymer **2** revealed a significant increase in D_h as [**2**] increased from 0.1 to 2 mg/mL (Figure S24). Meanwhile, assemblies of cyclic-linear graft copolymer **1i** revealed very little difference in D_h over this concentration range (Figure S24). Assemblies of **1i** and **2** were also monitored by DLS over time to gauge kinetic stability. After 48 h, assemblies of linear-linear graft copolymer **2** had disassembled to afford unimers with a D_h of *ca.* 7.5 nm (Figure 2). In contrast, assemblies of cyclic-linear graft copolymer **1** remained stable over a period of weeks; with no change in D_h or dispersity (Figure 2). SEC analysis confirmed the absence of graft copolymer degradation during this time period (Figure S25); therefore disassembly of linear-linear graft copolymer **2** under these conditions must result from poor particle stability and not polymer degradation. In combination, these findings strongly suggest that cyclic and linear polymers form assemblies of differing stability. Indeed, our results suggest that assemblies of cyclic-linear graft copolymer **1i** possess both greater thermodynamic and kinetic stability than assemblies of linear-linear graft copolymer **2**.

Table 1. Characterization data for self-assemblies of cyclic-linear and linear-linear PNAM graft copolymers **1i** and **2**.

Polymer	$D_{h \text{ (direct dissolution)}}$/nm (PD)[a]	$D_{h \text{ (solvent switch)}}$/nm (PD)[a]	$D_{h \text{ (thin film hydration)}}$/nm (PD)[a]	D_{ave}[b] /nm	R_g[c] /nm	cmc[d] /g·L^{-1}
1i - cyclic	170 (0.15)	170 (0.56)	150 (0.28)	207	75	0.09
2 - linear	200 (0.36)	115 (0.66)	7.1 (0.61)	-	140	0.23

[a]Determined by DLS analysis, D_h is for number average solution diameters. [b]Determined by cryo-TEM analysis from the counting of 50 particles, assemblies prepared by direct dissolution technique. [c]Determined by SAXS analysis, assemblies prepared by direct dissolution technique. [d]Determined by fluorescence spectroscopy using pyrene as the fluorescent probe, assemblies prepared by direct dissolution technique.

Small angle X-ray scattering (SAXS) and cryogenic transmission electron microscopy (cryo-TEM) were undertaken to gain further insight into the size and morphology of the graft copolymer assemblies (Figure 2 and S26). The SAXS profiles (at 0.5 mg/mL) of both the cyclic-linear and linear-linear graft copolymers exhibited the same pattern, with a plateau region at medium q values and up-turn at low q values (Figure 2). The Guinier-Porod model was used to fit the SAXS data excluding high q values. In agreement with particle size determined by DLS analysis, an R_g of 75 nm was calculated for cyclic-linear graft copolymer **1i**, and an R_g of 140 nm was found for linear-linear graft copolymer **2**. As was also observed by DLS analysis, the linear-linear graft exhibited a significantly larger dispersity than the cyclic-linear graft copolymer. Meanwhile, a Guinier plot (ln $I(q)$ *vs* q^2) was used to fit the SAXS data excluding the low q range, which gave R_g values of 3.7 and 3.3 nm for cyclic-linear and linear-linear graft copolymers **1i** and **2** respectively (Figure 2). As both large aggregates and unimers were observed in the linear-linear graft copolymer **2** by SAXS analysis, we suggest that a mixture of both is present in solution, indicative of a highly dynamic system. Cryo-TEM of cyclic-linear graft copolymer **1i** at 2 mg/mL revealed large spherical structures with an average diameter of 207 ± 61 nm, in agreement with DLS and SAXS analyses (Figure S26). Poor image contrast resulted from the high hydrophilic content of the assemblies and solvation of the PNAM corona. Cryo-TEM of linear-linear graft

15

copolymer **2** was attempted on numerous occasions, however no assemblies were observed, further suggestive of poor particle stability.
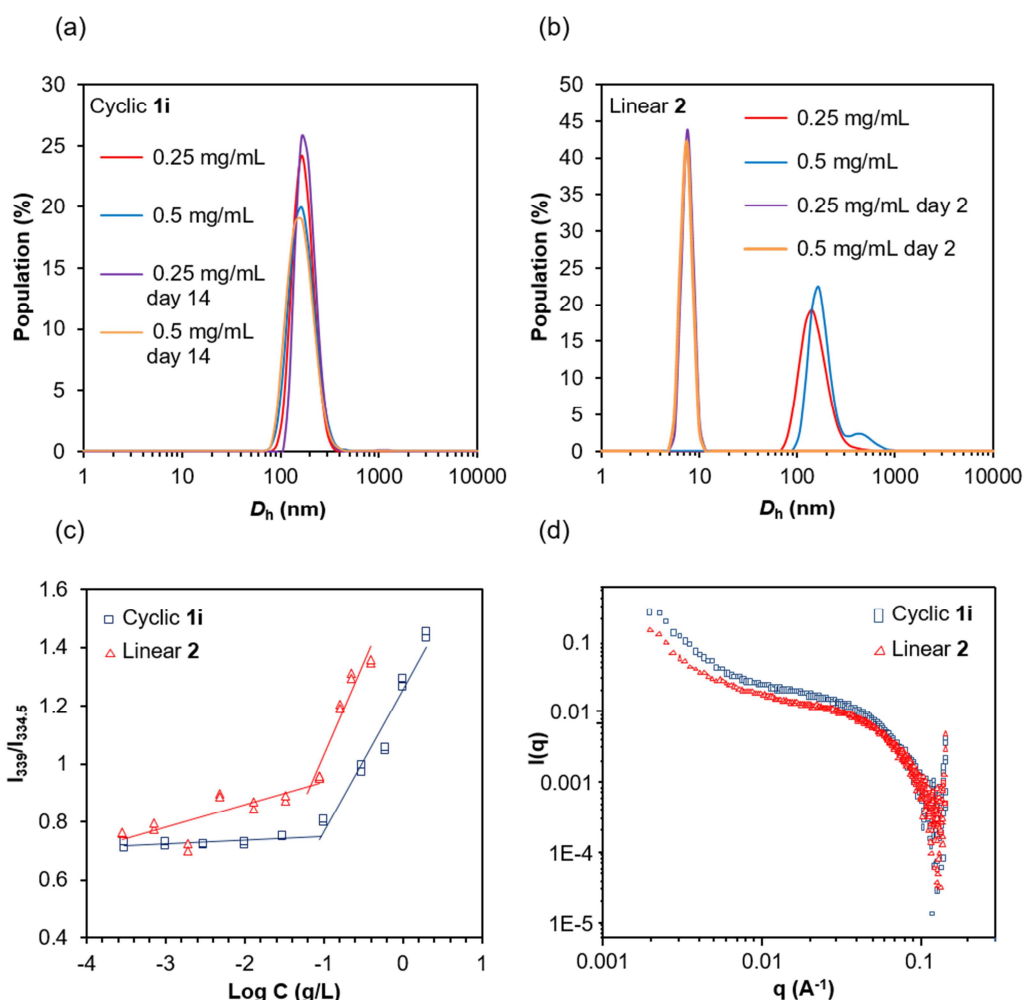

Figure 2. DLS analysis showing assembly size for cyclic-linear and linear-linear PNAM graft copolymers **1i** (a) and **2** (b) prepared *via* direct dissolution and their stability over time. (c) Concentration dependence of pyrene $I_{339}/I_{334.5}$ intensity ratio for assemblies **1i** and **2**. (d) SAXS profiles for assemblies of **1i** and **2** at 0.5 mg/mL.

Inspired by the observed differences in particle stability between assemblies of cyclic-linear and linear-linear graft copolymers, we envisaged that a change in polymer topology, from cyclic to linear, could be exploited as a trigger for particle disassembly. Such a method of disassembly would avoid non-specific, random polymer degradation and the formation of side-products as the disassembled polymer and original polymer vary only in topology. Cyclic-linear graft copolymer **1i** contains a disulfide moiety, which upon reduction induces

16

cleavage of the cyclic polymer backbone (Figure 1). We reasoned that the relative instability of the resulting assemblies of linear graft copolymer **3** would result in particle disassembly. To test this hypothesis, the *in vivo* reducing agent $_L$-glutathione (GSH) was added to a solution of aggregates of cyclic-linear graft copolymer **1i** (0.5 mg/mL, D_h = 170 nm). At intracellular concentrations of GSH (1-10 mM), DLS analysis after 16 h revealed the complete loss of large self-assembled structures and the presence of only very small species with solution diameters that correspond to unimers (D_h = 7.4 nm, PD = 0.46) (Figure 3a); consistent with backbone cleavage to yield a linear graft copolymer, followed by disassembly of the relatively unstable particles. The newly formed linear graft copolymer **3** remained as a unimer and did not reassemble over time as determined by DLS analysis. Meanwhile, assemblies of cyclic-linear graft copolymer **1i** in the presence of extracellular levels of GSH (1-10 μM) were observed to remain intact by DLS and did not disassemble over time (Figure S27). The transition from cyclic-linear graft copolymer aggregates to linear graft copolymer unimers was further studied by SAXS analysis over time and confirmed the disassembly of the particle under intracellular reducing conditions (Figure S27). Thus, as hypothesized, disulfide cleavage and particle disassembly are dependent on GSH concentration, which provides the opportunity for utilization of these constructs in specific triggered particle disassembly in intracellular environments.

To confirm that the topology switch is the key trigger for disassembly, a second responsive linker was explored to provide a second topology switching nanoparticle. To achieve this an acid-sensitive acetal linker was designed and introduced as a cleavable moiety in the cyclic polymer structure, to give **1ii**. The cyclic polymer based assembly **1ii** (0.5 mg/mL) was incubated in a solution at pH 4.0 for 100 h and degradation was monitored via DLS analysis. As expected, disassembly of the structure (with a decrease in particle size of 210 nm to 6.5 nm) was observed after 100 h of incubation under these conditions, showing

17

that the topology change, from cyclic to linear, is independent of the cleavable linker selected

or the conditions used (Figure 3c). Furthermore, when a non-responsive linker was used for

the cyclization (to afford polymer **1iii**), the topology switch from cyclic to linear did not

occur, as no change in size was observed by DLS analysis upon incubation with 10 mM GSH

(Figure 3b), while evidence of an increase in particle size, due to swelling of the assemblies,

rather than disassembly was observed upon a reduction in pH (Figure 3d). This confirms that

the topology change of the backbone from cyclic to linear (through incorporation of a

cleavable linker) is required for nanoparticle disassembly.
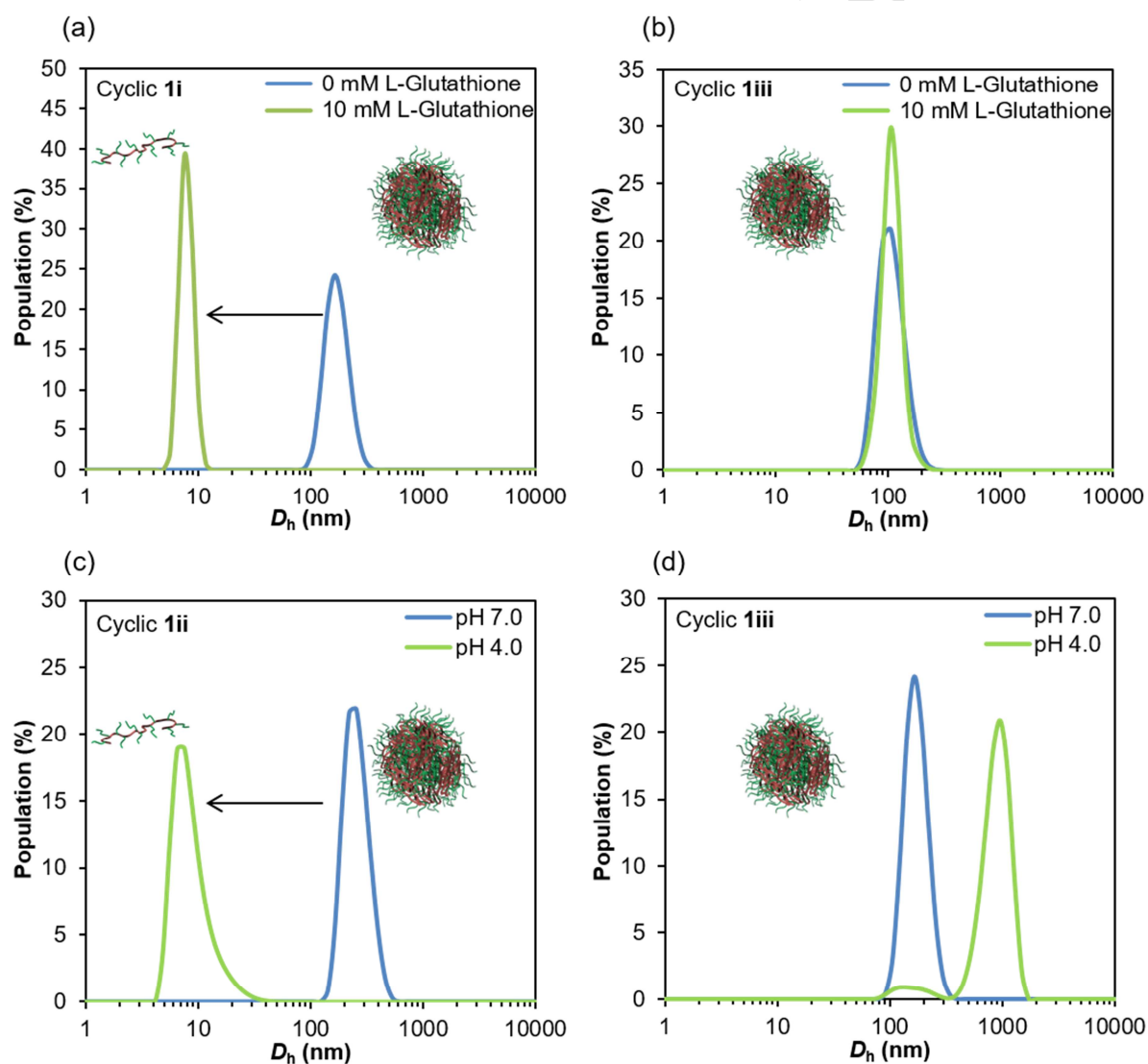
Figure 3. Aggregate disassembly triggered by disulfide cleavage of **1i** with 10 mM L-glutathione monitored by DLS before and 16 h after addition of GSH (a) and acetal cleavage

of **1ii** with 0.1 mM HCl at pH 4.0 before and 100 h after addition of HCl (c), compared to non-responsive linker **1iii** at the same conditions (b and d). D_h is volume average solution diameter.

To demonstrate the applicability of this stimuli triggered topology switch for clinical and biological applications, we firstly tested the cytotoxicity of our cyclic-linear and linear-linear graft copolymers and their ability to be internalized by cancer cells. A549 cells were selected for this study as a model cancer cell line with reported intracellular glutathione concentration higher than normal cells[39-41]. A549 (cancer lung fibroblasts) were incubated with increasing concentrations of cyclic-linear and linear-linear graft copolymers (from 0 to 2 mg/mL), and they showed a viability higher than 95% even at the highest concentration used (Figure S28), confirming the good cytocompatibility of the polymers. Furthermore, by encapsulating a fluorescent dye (BODIPY-FL) in both cyclic and linear polymer-based assemblies, we were able to track the particle's uptake by A549 cells. All cyclic-linear graft copolymer **1** (**1i - 1iii**) and linear-linear copolymer **2** assemblies (0.1 mg/mL) were internalized by A549 within 4 h of incubation (Figure 4, and S29-30). However, when the linear assemblies **2** were incubated with A549 for 4 h, the fluorescent dye was found to remain as a precipitate on the glass slide even after extensive washings with PBS (Figure 4). This behavior was only observed with the linear-based assembly and not with any of the cyclic-linear graft copolymers, suggesting the linear-linear polymer disassembles much quicker than its cyclic-based counterpart. This result correlates well with our observation on the difference in stability of the cyclic and linear assemblies' using scattering methods.

19
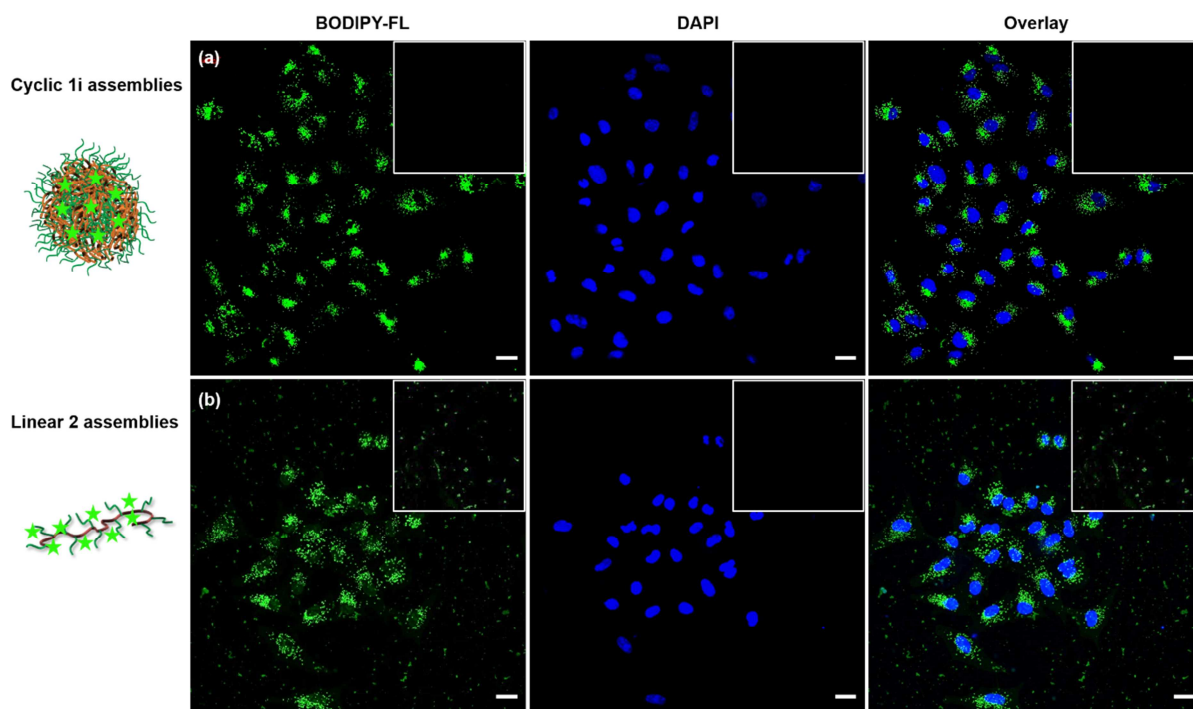
Figure 4. Internalization of cyclic **1i** assemblies (a) and linear **2** assemblies (b) encapsulating Bodipy-FL (green) by A549 cells. (Inset, top right corner) Expansion of the image highlighting the absence (a) or presence (b) of precipitated dye on the glass slide. Images were taken after 4 h of incubation with the assemblies. Cell nuclei (blue) are stained with DAPI. Scale bar = 20 µm.

Finally, to further exploit the scope of our topology-directed disassembly we loaded the assemblies of linear-linear and cyclic-linear NAM graft copolymers with an anti-cancer drug, camptothecin. Encapsulation efficiency (EE) was calculated as 70% for the cyclic-linear graft copolymers and 5% for the linear-linear graft copolymer assemblies, with a drug loading of 0.14 mg of drug/1 mg of cyclic polymer and 0.01 mg drug/1 mg of linear polymer. Little variation was observed in encapsulation efficiency using the three different cyclic polymers, when 20% drug:polymer feeding ratio was used. The lower EE obtained for the linear assemblies can be explained by their lower stability and tendency to disassemble over time. A549 cells were incubated with both cyclic-linear (**1i - 1iii**) and linear-linear, **2**, camptothecin loaded assemblies to investigate the effect of cleavage of the responsive linker, with subsequent release of the drug, upon uptake and exposure to the intracellular environment,

would have on the viability of the cancer cell line. Under these conditions, we confirmed the presence of aggregates of around 100 nm in diameter (Figure S31).

As expected, a higher decrease in viability over time was observed when A549 cells were incubated with the cyclic-linear graft polymers containing a responsive linker (cyclic **1i** and **1ii**) compared to the cyclic-linear graft polymer with the non-responsive linker (**1iii**), with a viability of 16 ± 3.0%, 35 ± 2.5% and 73 ± 8.7% for cyclic **1i**, cyclic **1ii**, and cyclic **1iii**, respectively, when the camptothecin concentration is 250 nM (Figure 5 and S32). However, it should be noted that cyclic **1iii**, containing the non-responsive linker, does induce cytotoxicity over time, with the cell viability decreasing below 40% after 72 h, when campothecin is encapsulated (Figure S32). In order to investigate if the cytotoxicity is a consequence of glutathione triggered release, a release study was conducted using 10 mM GSH as external stimulus. A 65% camptothecin release was observed from cyclic **1i**, while no release was detected from cyclic **1iii** (Figure S33). These data are in good agreement with the DLS study shown in Figure 3, where no disassembly was observed for cyclic **1iii** using 10 mM GSH. Therefore, the release of camptothecin from cyclic **1iii** could be ascribed to either swelling, which indeed occurs at acidic pH (Figure 3d), or degradation of the polymer backbone in the cell environment and subsequent release, which has been reported before for polymeric nanoparticles with a degradable backbone[42].

In contrast, when A549 were incubated with the same concentration of linear-linear copolymer assemblies, **2**, polymer viability was found to be higher than 95%, as a consequence of the lower amount of drug encapsulated (Figure S34).

21
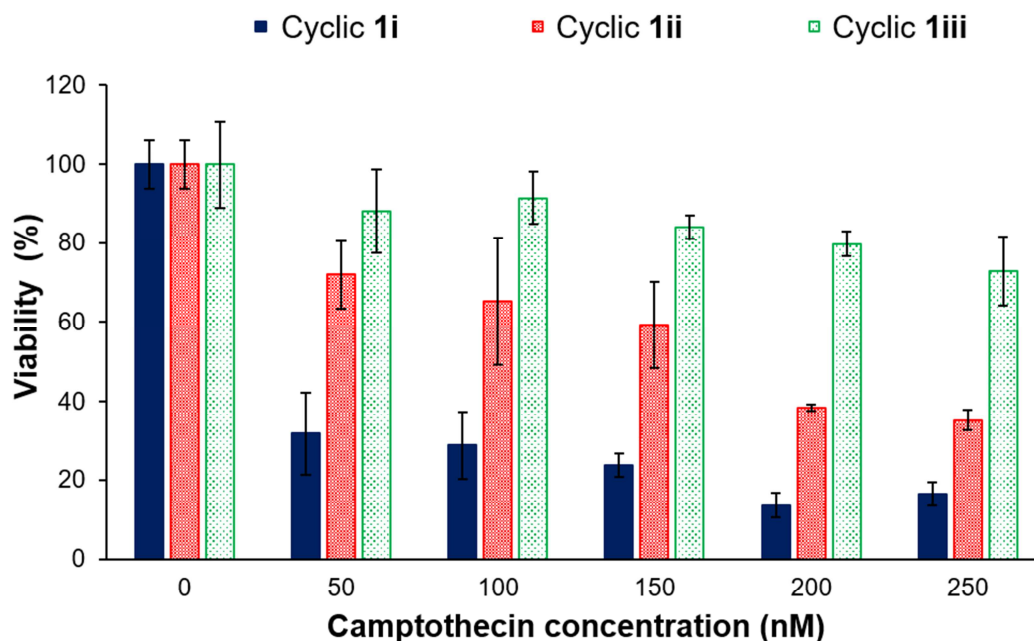
Figure 5. Viability of A549 cells incubated for 24 h with increasing concentrations (from 0 to 250 nM) of camptothecin encapsulated in the cyclic-linear graft copolymer assemblies (**1i**, **1ii**, and **1iii**).

Conclusions

Herein, we have shown that self-assembled nanoparticles that are comprised of cyclic-linear graft copolymers are significantly more stable, and are better able to encapsulate hydrophobic molecules, than their directly analogous (same chemistry) linear-linear equivalents. Subsequently, we have exploited the difference in assembly stability by switching between polymer topologies to direct the triggered disassembly of polymer nanoparticle constructs. In turn, we show that this approach can be used as to trigger the release of an anti-cancer drug *in vitro* using intracellular stimuli, such as intracellular glutathione concentration and acidic pH, to trigger the change in polymer topology.

This study highlights, for the first time, that careful design of polymer topology and chemistry can be used to design novel delivery vehicles capable of triggered drug release. Indeed, we hypothesize that the cleavage of single bond within the polymer chain, which leads only to a change in topology of the core of the graft copolymer from cyclic to linear and subsequently facilitates nanoparticle disassembly, represents a new mechanism for controlled

22

release. Moreover, the simple change of one bond within the polymer structure ensures that the bulk of the chemical structure, molar mass and solubility are largely the same for both polymers before and after the delivery event which in turn should ensure that toxicity and retention characteristics of the polymer are unaltered. We believe that this is the first time that such a topology-driven switch has been reported and could have profound implications on the field of nanoparticle-mediate drug delivery.

Acknowledgements

References

[1] K. Endo, Synthesis and Properties of Cyclic Polymers. In New Frontiers in Polymer Synthesis, S. Kobayashi, Ed. Springer Berlin Heidelberg: (2008) 217, 121-183.
[2] Z. Jia, M. J. Monteiro, Cyclic polymers: Methods and strategies, J. Polym. Sci. A 50 (11) (2012) 2085-2097.
[3] H. R. Kricheldorf, Cyclic polymers: Synthetic strategies and physical properties, J. Polym. Sci., Part A: Polym. Chem. 48 (2010) 251-284.
[4] B. A. Laurent, S. M. Grayson, Synthetic approaches for the preparation of cyclic polymers, Chem. Soc. Rev. 38 (8) (2009) 2202-2213.
[5] X.-Y. Tu, M.-Z. Liu, H. Wei, Recent progress on cyclic polymers: Synthesis, bioproperties, and biomedical applications, J. Polym. Sci. A 54 (11) (2016) 1447-1458.
[6] R. J. Williams, A. P. Dove, R. K. O'Reilly, Self-assembly of cyclic polymers, Polym. Chem. 6 (16) (2015) 2998-3008.
[7] T. Yamamoto, Y. Tezuka, Topological polymer chemistry: a cyclic approach toward novel polymer properties and functions, Polym. Chem. 2 (9) (2011) 1930-1941.
[8] T. Yamamoto, Y. Tezuka, Cyclic polymers revealing topology effects upon self-assemblies, dynamics and responses, Soft Matter 11 (38) (2015) 7458-7468.
[9] M. A. Cortez, W. T. Godbey, Y. Fang, M. E. Payne, B. J. Cafferty, K. A. Kosakowska, S. M. Grayson, The Synthesis of Cyclic Poly(ethylene imine) and Exact Linear Analogues: An Evaluation of Gene Delivery Comparing Polymer Architectures, J. Am. Chem. Soc. 137 (20) (2015) 6541-6549.

[10] H. Wei, D. S. H. Chu, J. Zhao, J. A. Pahang, S. H. Pun, Synthesis and Evaluation of Cyclic Cationic Polymers for Nucleic Acid Delivery, ACS Macro Lett. 2 (12) (2013) 1047-1050.

[11] N. Nasongkla, B. Chen, N. Macaraeg, M. E. Fox, J. M. J. Fréchet, F. C. Szoka, Dependence of Pharmacokinetics and Biodistribution on Polymer Architecture: Effect of Cyclic versus Linear Polymers, J. Am. Chem. Soc. 131 (11) (2009) 3842-3843.

[12] C. E. Wang, H. Wei, N. Tan, A. J. Boydston, S. H. Pun, Sunflower Polymers for Folate-Mediated Drug Delivery, Biomacromolecules 17 (1) (2016) 69-75.

[13] Y. Wang, R. Zhang, N. Xu, F.-S. Du, Y.-L. Wang, Y.-X. Tan, S.-P. Ji, D.-H. Liang, Z.-C. Li, Reduction-Degradable Linear Cationic Polymers as Gene Carriers Prepared by Cu(I)-Catalyzed Azide–Alkyne Cycloaddition, Biomacromolecules 12 (1) (2011) 66-74.

[14] B. Zhang, H. Zhang, Y. Li, J. N. Hoskins, S. M. Grayson, Exploring the Effect of Amphiphilic Polymer Architecture: Synthesis, Characterization, and Self-Assembly of Both Cyclic and Linear Poly(ethylene gylcol)-b-polycaprolactone, ACS Macro Lett. 2 (10) (2013) 845-848.

[15] R. Borsali, E. Minatti, J.-L. Putaux, M. Schappacher, A. Deffieux, P. Viville, R. Lazzaroni, T. Narayanan, From "Sunflower-like" Assemblies toward Giant Wormlike Micelles, Langmuir 19 (1) (2002) 6-9.

[16] E. Minatti, R. Borsali, M. Schappacher, A. Deffieux, V. Soldi, T. Narayanan, J.-L. Putaux, Effect of Cyclization of Polystyrene/Polyisoprene Block Copolymers on Their Micellar Morphology, Macromol. Rapid Commun. 23 (16) (2002) 978-982.

[17] E. Minatti, P. Viville, R. Borsali, M. Schappacher, A. Deffieux, R. Lazzaroni, Micellar Morphological Changes Promoted by Cyclization of PS-b-PI Copolymer: DLS and AFM Experiments, Macromolecules 36 (11) (2003) 4125-4133.

[18] S. Honda, T. Yamamoto, Y. Tezuka, Topology-Directed Control on Thermal Stability: Micelles Formed from Linear and Cyclized Amphiphilic Block Copolymers, J. Am. Chem. Soc. 132 (30) (2010) 10251-10253.

[19] S. Honda, T. Yamamoto, Y. Tezuka, Tuneable enhancement of the salt and thermal stability of polymeric micelles by cyclized amphiphiles, Nat. Commun. 4 (2013) 1574.

[20] K. Loomis, K. McNeeley, R. V. Bellamkonda, Nanoparticles with targeting, triggered release, and imaging functionality for cancer applications, Soft Matter 7 (3) (2011) 839-856.

[21] M. Caldorera-Moore, N. Guimard, L. Shi, K. Roy, Designer nanoparticles: incorporating size, shape and triggered release into nanoscale drug carriers, Expert Opin. Drug Deliv. 7 (4) (2010) 479-495.

[22] H. Wu, J. Dong, X. Zhan, H. Yang, Y. Zhao, S. Zhu, G. Wang, Triple stimuli-responsive crosslinked polymeric nanoparticles for controlled release, RSC Adv. 4 (67) (2014) 35757-35761.

[23] S. Lappe, D. Mulac, K. Langer, Polymeric nanoparticles – Influence of the glass transition temperature on drug release, Int. J. Pharm 517 (1) (2017) 338-347.

[24] J. Dong, R. Zhang, H. Wu, X. Zhan, H. Yang, S. Zhu, G. Wang, Polymer Nanoparticles for Controlled Release Stimulated by Visible Light and pH, Macromol. Rapid Commun. 35 (14) (2014) 1255-1259.

[25] R. Cheng, F. Feng, F. Meng, C. Deng, J. Feijen, Z. Zhong, Glutathione-responsive nano-vehicles as a promising platform for targeted intracellular drug and gene delivery, J. Control. Release 152 (1) (2011) 2-12.

[26] R. Mo, Z. Gu, Tumor microenvironment and intracellular signal-activated nanomaterials for anticancer drug delivery, Mater. Today 19 (5) (2016) 274-283.

[27] J. F. Quinn, M. R. Whittaker, T. P. Davis, Glutathione responsive polymers and their application in drug delivery systems, Polym. Chem. (2017) DOI:10.1039/C1036PY01365A.

[28] R. S. Navath, Y. E. Kurtoglu, B. Wang, S. Kannan, R. Romero, R. M. Kannan, Dendrimers-drug conjugates for tailored intracellular drug release based on glutathione levels, Bioconjugate Chem. 19 (12) (2008) 2446-2455.

[29] K. Fukushima, R. C. Pratt, F. Nederberg, J. P. K. Tan, Y. Y. Yang, R. M. Waymouth, J. L. Hedrick, Organocatalytic Approach to Amphiphilic Comb-Block Copolymers Capable of Stereocomplexation and Self-Assembly, Biomacromolecules 9 (11) (2008) 3051-3056.

[30] R. J. Williams, R. K. O'Reilly, A. P. Dove, Degradable graft copolymers by ring-opening and reverse addition-fragmentation chain transfer polymerization, Polym. Chem. 3 (8) (2012) 2156-2164.

[31] M. Malkoch, K. Schleicher, E. Drockenmuller, C. J. Hawker, T. P. Russell, P. Wu, V. V. Fokin, Structurally Diverse Dendritic Libraries: A Highly Efficient Functionalization Approach Using Click Chemistry, Macromolecules 38 (9) (2005) 3663-3678.

[32] R. J. Williams, A. Pitto-Barry, N. Kirby, A. P. Dove, R. K. O'Reilly, Cyclic Graft Copolymer Unimolecular Micelles: Effects of Cyclization on Particle Morphology and Thermoresponsive Behavior, Macromolecules 49 (7) (2016) 2802-2813.

[33] A. B. J. Withey, G. Chen, T. L. U. Nguyen, M. H. Stenzel, Macromolecular Cobalt Carbonyl Complexes Encapsulated in a Click-Cross-Linked Micelle Structure as a Nanoparticle To Deliver Cobalt Pharmaceuticals, Biomacromolecules 10 (12) (2009) 3215-3226.

[34] E. J. O'Neil, K. M. DiVittorio, B. D. Smith, Phosphatidylcholine-Derived Bolaamphiphiles via Click Chemistry, Org. Lett. 9 (2) (2007) 199-202.

[35] J. R. Thomas, X. Liu, P. J. Hergenrother, Size-Specific Ligands for RNA Hairpin Loops, J. Am. Chem. Soc. 127 (36) (2005) 12434-12435.

[36] E. D. Goddard-Borger, R. V. Stick, An Efficient, Inexpensive, and Shelf-Stable Diazotransfer Reagent: Imidazole-1-sulfonyl Azide Hydrochloride, Org. Lett. 9 (19) (2007) 3797-3800.

[37] H. He, Y. Bai, J. Wang, Q. Deng, L. Zhu, F. Meng, Z. Zhong, L. Yin, Reversibly Cross-Linked Polyplexes Enable Cancer-Targeted Gene Delivery via Self-Promoted DNA Release and Self-Diminished Toxicity, Biomacromolecules 16 (4) (2015) 1390-1400.

[38] W. A. Prütz, J. Butler, E. J. Land, Photocatalytic and Free Radical Interactions of the HeterocyclicN-Oxide Resazurin with NADH, GSH, and Dopa, Archives of Biochemistry and Biophysics 327 (2) (1996) 239-248.

[39] M. P. Gamcsik, M. S. Kasibhatla, S. D. Teeter, O. M. Colvin, Glutathione levels in human tumors, Biomarkers 17 (8) (2012) 671-691.

[40] N. Traverso, R. Ricciarelli, M. Nitti, B. Marengo, A. L. Furfaro, M. A. Pronzato, U. M. Marinari, C. Domenicotti, Role of Glutathione in Cancer Progression and Chemoresistance, Oxidative Medicine and Cellular Longevity 2013 (2013) 972913.

[41] A. Russo, W. DeGraff, N. Friedman, J. B. Mitchell, Selective Modulation of Glutathione Levels in Human Normal versus Tumor Cells and Subsequent Differential Response to Chemotherapy Drugs, Cancer Research 46 (6) (1986) 2845.

[42] K. S. Soppimath, T. M. Aminabhavi, A. R. Kulkarni, W. E. Rudzinski, Biodegradable polymeric nanoparticles as drug delivery devices, J. Control. Release 70 (1) (2001) 1-20.